

# FRECaS: EFFICIENT HIGHER-RESOLUTION IMAGE GENERATION VIA FREQUENCY-AWARE CASCADED SAMPLING

Zhengqiang Zhang<sup>1,2</sup>, Ruihuang Li<sup>1,2</sup>, Lei Zhang<sup>1,2,\*</sup>

<sup>1</sup>The Hong Kong Polytechnic University    <sup>2</sup>OPPO Research Institute

zhengqiang.zhang@connect.polyu.hk, cslzhang@comp.polyu.edu.hk

## ABSTRACT

While image generation with diffusion models has achieved a great success, generating images of higher resolution than the training size remains a challenging task due to the high computational cost. Current methods typically perform the entire sampling process at full resolution and process all frequency components simultaneously, contradicting with the inherent coarse-to-fine nature of latent diffusion models and wasting computations on processing premature high-frequency details at early diffusion stages. To address this issue, we introduce an efficient **Frequency-aware Cascaded Sampling** framework, **FreCaS** in short, for higher-resolution image generation. FreCaS decomposes the sampling process into cascaded stages with gradually increased resolutions, progressively expanding frequency bands and refining the corresponding details. We propose an innovative frequency-aware classifier-free guidance (FA-CFG) strategy to assign different guidance strengths for different frequency components, directing the diffusion model to add new details in the expanded frequency domain of each stage. Additionally, we fuse the cross-attention maps of previous and current stages to avoid synthesizing unfaithful layouts. Experiments demonstrate that FreCaS significantly outperforms state-of-the-art methods in image quality and generation speed. In particular, FreCaS is about  $2.86\times$  and  $6.07\times$  faster than ScaleCrafter and DemoFusion in generating a  $2048\times 2048$  image using a pre-trained SDXL model and achieves an  $FID_b$  improvement of 11.6 and 3.7, respectively. FreCaS can be easily extended to more complex models such as SD3. The source code of FreCaS can be found at <https://github.com/xtudbxk/FreCaS>.

## 1 INTRODUCTION

In recent years, diffusion models, such as Imagen (Saharia et al., 2022), SDXL (Podell et al., 2023), PixelArt- $\alpha$  (Chen et al., 2023) and SD3 Esser et al. (2024), have achieved a remarkable success in generating high-quality natural images. However, these models face challenges in generating very high resolution images due to the increased complexity in high-dimensional space. Though efficient diffusion models, including ADM (Dhariwal & Nichol, 2021), CascadedDM (Ho et al., 2022) and LDM (Rombach et al., 2022), have been developed, the computational burden of training diffusion models from scratch for high-resolution image generation remains substantial. As a result, popular diffusion models, such as SDXL (Podell et al., 2023) and SD3 (Esser et al., 2024), primarily focus on generating  $1024 \times 1024$  resolution images. It is thus increasingly attractive to explore training-free strategies for generating images at higher resolutions, such as  $2048 \times 2048$  and  $4096 \times 4096$ , using pre-trained diffusion models.

MultiDiffusion (Bar-Tal et al., 2023) is among the first works to synthesize higher-resolution images using pre-trained diffusion models. However, it suffers from issues such as object duplication, which largely reduces the image quality. To address these issues, Jin et al. (2024) proposed to manually adjust the scale of entropy in the attention operations. He et al. (2023) and Linjiang Huang (2024) attempted to enlarge the receptive field by replacing the original convolutional layers with strided ones, while Zhang et al. (2023) explicitly resizes the intermediate feature maps to match the train-

---

\*Corresponding author.

ing size. Du et al. (2024) and Lin et al. (2024) took a different strategy by generating a reference image at the base resolution and then using it to guide the whole sampling process at higher resolutions. Despite the great advancements, these methods still suffer from significant inference latency, hindering their broader applications in real world.

In this paper, we propose an efficient **F**requency-aware **C**ascaded **S**ampling framework, namely **FreCaS**, for training-free higher-resolution image generation. Our proposed FreCaS framework is based on the observation that latent diffusion models exhibit a coarse-to-fine generation manner in the frequency domain. In other words, they first generate low-frequency contents in early diffusion stages and gradually generate higher-frequency details in later stages. Leveraging this insight, we generate higher-resolution images through multiple stages of increased resolutions, progressively synthesizing details of increased frequencies. FreCaS avoids unnecessary computations during the early diffusion stages as high-frequency details are not yet required.

In the latent space, the image representation expands its frequency range as the resolution increases. To encourage detail generation within the expanded frequency band, we introduce a novel frequency-aware classifier-free guidance (FA-CFG) strategy, which prioritizes newly introduced frequency components by assigning them higher guidance strengths in the sampling process. Specifically, we decompose both unconditional and conditional denoising scores into two parts: low-frequency component, which captures content from earlier stages, and high-frequency component, which corresponds to the newly increased frequency band. FA-CFG applies the classifier-free guidance to different frequency components with different strengths, and outputs the final denoising score by combining the adjusted components. The FA-CFG strategy can synthesize much clear details while maintaining computational efficiency. Additionally, to alleviate the issue of unfaithful layouts, such as duplicated objects mentioned in Jin et al. (2024), we reuse the cross-attention maps (CA-maps) from the previous stage, which helps maintaining consistency in image structure across different stages and ensuring more faithful object representations.

In summary, our main contributions are as follows:

- We propose FreCaS, an efficient frequency-aware cascaded sampling framework for training-free higher-resolution image generation. FreCaS leverages the coarse-to-fine nature of the latent diffusion process, thereby reducing unnecessary computations associated with processing premature high-frequency details.
- We design a novel FA-CFG strategy, which assigns different guidance strengths to components of different frequencies. This strategy enables FreCaS to focus on generating contents of newly introduced frequencies in each stage, and hence synthesize clearer details. In addition, we fuse the CA-maps of previous stage and current stage to maintain a consistent image layouts across stages.
- We demonstrate the efficiency and effectiveness of FreCaS through extensive experiments conducted on various pretrained diffusion models, including SD2.1, SDXL and SD3, validating its broad applicability and versatility.

## 2 RELATED WORKS

### 2.1 DIFFUSION MODELS

Diffusion models have gained significant attentions due to their abilities to generate high-quality natural images. Ho et al. (2020) pioneered the use of a variance-preserving diffusion process to bridge the gap from natural images to pure noises. Dhariwal & Nichol (2021) exploited various network architectures and achieved superior image quality than contemporaneous GAN models. Ho & Salimans (2022) introduced a novel classifier-free guidance strategy that attains both generated image quality and diversity. However, the substantial model complexity makes high-resolution image synthesis challenging. Ho et al. (2022) proposed a novel cascaded framework that progressively increases image resolutions. Rombach et al. (2022) performed the diffusion process in the latent space of a pre-trained autoencoder, enabling high-resolution image synthesis with reduced computational cost. (Esser et al., 2024) presented SD3, which employs the rectified flow matching (Lipman et al., 2022; Liu et al., 2022) at the latent space and demonstrates superior performance. Despite the great progress, it still requires substantial efforts to train a high-resolution diffusion model from scratch. Therefore, training-free higher-resolution image synthesis attracts increasing attentions.

## 2.2 TRAINING-FREE HIGHER-RESOLUTION IMAGE SYNTHESIS

A few methods have been developed to leverage pre-trained diffusion models to generate images of higher resolutions than the training size. MultiDiffusion (Bar-Tal et al., 2023) is among the first methods to bind multiple diffusion processes into one unified framework and generates seamless higher-resolution images. However, the results exhibit unreasonable image structures such as duplicated objects. AttnEntropy (Jin et al., 2024) alleviates this problem by re-normalizing the entropy of attention blocks during sampling. On the other hand, ScaleCrafter (He et al., 2023) and FouriScale (Linjiang Huang, 2024) expand the receptive fields of pre-trained networks to match higher inference resolutions, thereby demonstrating improved image quality. HiDiffusion (Zhang et al., 2023) dynamically adjusts the feature sizes to match the training dimensions. DemoFusion (Du et al., 2024) and AccDiffusion (Lin et al., 2024) first generate a reference image at the standard resolution and then use this image to guide the generation of images at higher resolutions. Despite their success, the above mentioned approaches neglect the coarse-to-fine nature of image generation and generate image contents of all frequencies simultaneously, resulting in long inference latency and limiting their broader applications.

To address this issue, we propose an efficient FreCaS framework for training-free higher-resolution image synthesis. FreCaS divides the entire sampling process into stages of increasing resolutions, gradually synthesizing components of different frequency bands, thereby reducing the unnecessary computation of handling premature high-frequency details in early sampling stages. It is worth noting that DemoFusion (Du et al., 2024) employs a progressive upscaling scheme that may appear similar to our approach. However, there exist fundamental differences: DemoFusion utilizes the generated image at the base resolution as a reference to guide the entire sampling process at target resolution, whereas FreCaS continues the sampling process at higher resolutions. This distinction makes our method significantly more efficient than DemoFusion, achieving better image quality with largely reduced computations.

## 3 METHOD

This section presents the details of the proposed FreCaS framework, which leverages the coarse-to-fine nature of latent diffusion models and constructs a frequency-aware cascaded sampling strategy to progressively refine high-frequency details. We first introduce the notations and concepts that form the basis of our approach (see Section 3.1). Then, we delve into the key components of our method: FreCaS framework (see Section 3.2), FA-CFG strategy (see Section 3.3), and CA-maps re-utilization (see Section 3.4).

### 3.1 PRELIMINARIES

**Diffusion models.** Diffusion models (Ho et al., 2020; Dhariwal & Nichol, 2021) transform complex image distributions into the Gaussian distribution, and vice versa. They gradually inject Gaussian noises into the image samples, and then use a reverse process to remove noises from them, achieving image generation. Most recent diffusion models operate in the latent space and utilize a discrete timestep sampling process to synthesize images. Specifically, for a  $T$ -step sampling process, a latent noise  $z_T$  is drawn from a standard Gaussian distribution, and then iteratively refined through a few denoising steps until converged to the clean signal latent  $z_0$ . Finally, the natural image  $x$  is decoded from  $z_0$  using a decoder  $\mathcal{D}$ . The whole process can be written as follows:

$$z_T \sim \mathcal{N}(\mathbf{0}, \mathbf{I}) \rightarrow z_{T-1} \rightarrow \cdots \rightarrow z_1 \rightarrow z_0 \rightarrow x = \mathcal{D}(z_0). \quad (1)$$

For each denoising step, current works typically adopt the classifier-free guidance (CFG) (Ho & Salimans, 2022) to improve image quality. It predicts an unconditional denoising score  $\epsilon_{unc}$  and a conditional denoising score  $\epsilon_c$ . The final denoising score is obtained via a simple extra-interpolation process as  $\hat{\epsilon} = (1 - w) \cdot \epsilon_{unc} + w \cdot \epsilon_c$ , where  $w$  denotes the guidance strength.

**Resolution and frequency range.** The resolution of a latent  $z$  determines its sampling frequency (Rissanen et al., 2023), thereby influencing its frequency domain characteristics. Specifically, if a latent of unit length has a resolution of  $s \times s$ , its sampling frequency  $f_s$  can be defined as the number of samples per unit length, which is  $s$ . The Nyquist frequency is then obtained as

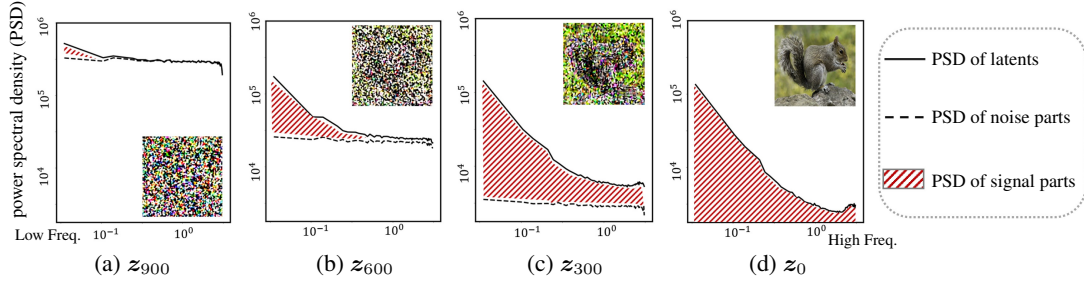


Figure 1: From (a) to (d), the sub-figures show the PSD curves of latents  $z_{900}$ ,  $z_{600}$ ,  $z_{300}$  and  $z_0$  of SDXL, respectively. One can see that the energy of synthesized clean signals (the red slashed regions) first emerges in the low-frequency band and gradually expands to high-frequency band.

$\frac{f_s}{2} = \frac{s}{2}$ . Therefore, the frequency of the latent  $z$  ranges from  $[0, \frac{s}{2}]$ . Reducing its resolution to  $s_l \times s_l$  narrows the frequency range to  $[0, \frac{s_l}{2}]$ . As a result, higher resolutions capture a broader frequency domain, while lower resolutions lead to a narrower frequency spectrum.

### 3.2 FREQUENCY-AWARE CASCADED SAMPLING

Pixel space diffusion models exhibit a coarse-to-fine behavior in the image synthesis process (Rissanen et al., 2023; Teng et al., 2024). In this section, we show that such a behavior is also exhibited for latent diffusion models during the sampling process, which inspires us to develop a frequency-aware cascaded sampling framework for generating higher-resolution images.

**PSD curves in latent space.** The power spectral density (PSD) is a powerful tool for analyzing the energy distribution of signals along the frequency spectrum. Rissanen et al. (2023) and Teng et al. (2024) have utilized PSD to study the behaviour of intermediate states in the pixel diffusion process. Here, we compute the PSD of the latent signals over a collection of 100 natural images using the pre-trained SDXL model (Podell et al., 2023). Figure 1 shows the PSD curves of  $z_{900}$ ,  $z_{600}$ ,  $z_{300}$  and  $z_0$ . The solid line denotes the PSD curve of intermediate noise corrupted latent, while the dashed line represents the PSD of Gaussian noise corrupted into the latent. The inner area between the two curves (marked with red slashes) indicates the energy of clean signal latent being synthesized. One can see that the clean image signals emerge from the low-frequency band (see  $z_{900}$  and  $z_{600}$ ) and gradually expand to the high-frequency band (see  $z_{300}$  and  $z_0$ ) during the sampling process. These observations confirm the coarse-to-fine nature of image synthesis in the latent diffusion process, where low-frequency content is generated first, followed by high-frequency details.

**Framework of FreCaS.** Based on the above observation, we developed an efficient FreCaS framework to progressively generate image contents of higher frequency bands, reducing unnecessary computations in processing premature high-frequency details in early diffusion stages. As shown in Figure 2(a), our FreCaS divides the entire  $T$ -step sampling process into  $N + 1$  stages of increasing resolutions. The initial stage performs the sampling process at the default training size  $s_0$  with a frequency range of  $[0, \frac{s_0}{2}]$ . Each of the subsequent stages increases the sampling size to its predecessor, gradually expanding the frequency domain. At the final stage, the latent reaches the target resolution  $s_N$ , achieving a full frequency range from 0 to  $\frac{s_N}{2}$ .

Specifically, we begin with a pure noise latent  $z_T^{s_0}$  at stage  $s_0$ , and iteratively perform reverse sampling until obtaining the last latent in this stage, denoted by  $z_L^{s_0}$ . Next, we transition  $z_L^{s_0}$  to the first latent, denoted by  $z_F^{s_1}$ , in next stage, as illustrated by the blue dashed arrow in Figure 2(a). This procedure is repeated until the latent feature reaches the target size, resulting in  $z_0^{s_N}$ . The final image  $x$  is obtained by applying the decoder to  $z_0^{s_N}$  so that  $x = \mathcal{D}(z_0^{s_N})$ . With such a sampling pipeline, FreCaS ensures a gradual refinement of details across coarse-to-fine scales, ultimately producing a high-quality and high-resolution image with minimum computations.

For the transition between two adjacent stages, we perform five steps to convert the last latent of previous stage  $z_L^{s_{i-1}}$  to the first latent of next stage  $z_F^{s_i}$ :

$$z_L^{s_{i-1}} \xrightarrow{\text{denoise}} \hat{z}_0^{s_{i-1}} \xrightarrow{\text{decode}} \hat{x}^{s_{i-1}} \xrightarrow{\text{interpolate}} \hat{x}^{s_i} \xrightarrow{\text{encode}} z_0^{s_i} \xrightarrow{\text{diffuse}} z_F^{s_i}, \quad (2)$$

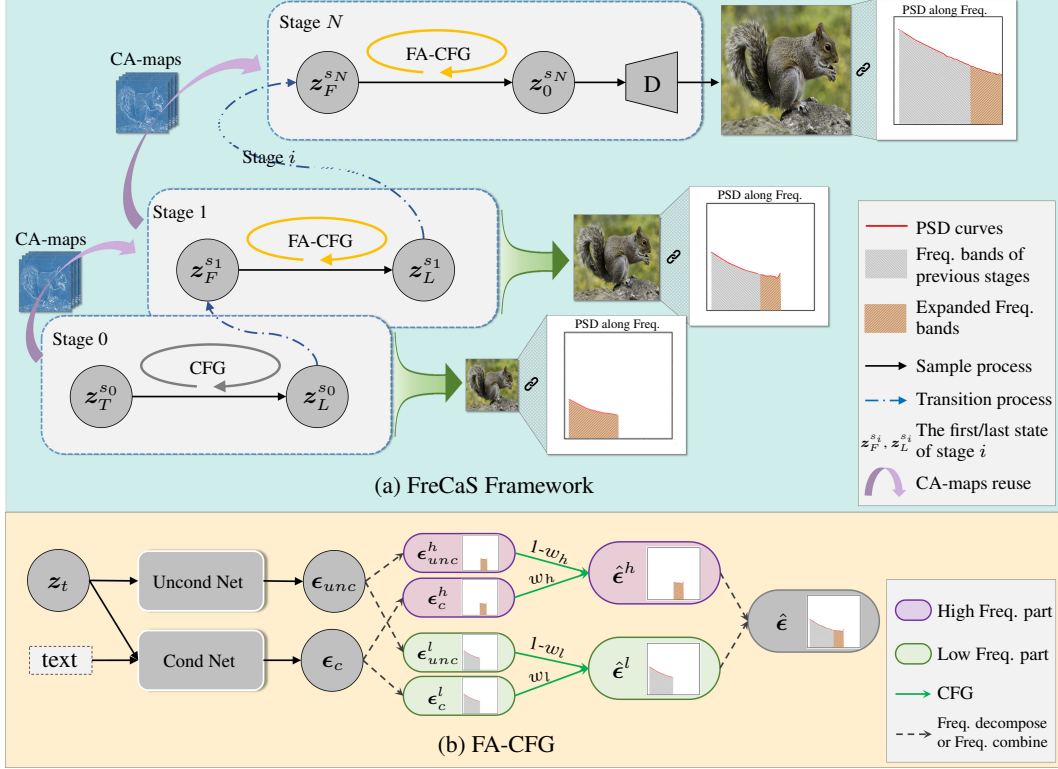


Figure 2: (a) The overall framework of FreCaS. The entire  $T$ -step sampling process is divided into  $N + 1$  stages of increasing resolutions and expanding frequency bands. FreCaS starts the sampling process at the training size and obtains the last latent  $z_L^{s_0}$  at that stage. Then, FreCaS continues the sampling from the first latent  $z_F^{s_1}$  at the next stage with a larger resolution and expanded frequency domain. This procedure is repeated until the final latent  $z_0^{s_N}$  at stage  $N$  is obtained. A decoder is then used to generate the final image. (b) FA-CFG strategy. We separate the original denoising scores into low-frequency and high-frequency components and assign a higher CFG strength to the high-frequency part. The two parts are then combined to obtain the final denoising score  $\hat{\epsilon}$ .

where “denoise” and “diffuse” are standard diffusion operations, “decode” and “encode” are performed using the decoder and encoder, respectively, and “interpolation” adjusts the resolutions using the bilinear interpolation. To determine the timestep of  $z_F^{s_i}$ , we follow previous works (Hoogeboom et al., 2023; Chen, 2023; Gu et al., 2023; Teng et al., 2024) to keep the signal-to-noise ratio (SNR) equivalence between  $z_L^{s_{i-1}}$  and  $z_F^{s_i}$ . Please refer to Appendix A for more details.

### 3.3 FA-CFG STRATEGY

Our FreCaS framework progressively transitions the latents to stages with higher resolutions and extended high-frequency bands. To ensure that the diffusion models focus more on generating contents of newly introduced frequencies, we propose a novel FA-CFG strategy, which assigns higher guidance strength to the new frequency components. In FreCaS, upon transitioning to stage  $s_i$ , the latent increases its resolution from  $s_{i-1}$  to the higher resolution  $s_i$ , thereby expanding the frequency band from  $[0, \frac{s_{i-1}}{2}]$  to  $[0, \frac{s_i}{2}]$ . This inspires us to divide the latents into two components: a low-frequency component ranging from  $[0, \frac{s_{i-1}}{2}]$  and a high-frequency component covering the frequency interval  $(\frac{s_{i-1}}{2}, \frac{s_i}{2}]$ . The former preserves the generated contents from previous stages, whereas the latter is reserved for the contents to be generated in this stage. Our goal is to encourage the diffusion models to generate natural details and textures in the newly expanded frequency band.

To achieve the above mentioned goal, we propose to perform CFG on the two frequency-aware parts with different guidance strengths. The entire process is illustrated in Figure 2(b). First, we obtain the unconditional denoising score  $\epsilon_{unc}$  and conditional denoising score  $\epsilon_c$  using the pre-trained diffusion network. Then, we split the scores into a low-frequency part and a high-frequency part. The former is extracted by downsampling the scores and then resizing them back, while the latter is

the residual by subtracting the low-frequency part from the original denoising scores. Subsequently, we apply the CFG strategy to the two parts with different weights. Specifically, for the low-frequency part, we assign the normal guidance strength  $w_l$ , while for the high-frequency part, we use a much higher weight  $w_h$  to prioritize content generation in this frequency band. The final denoising score is obtained by summing up the two parts. This process can be expressed as:

$$\hat{\epsilon} = \hat{\epsilon}^l + \hat{\epsilon}^h = (1 - w_l) \cdot \epsilon_{unc}^l + w_l \cdot \epsilon_c^l + (1 - w_h) \cdot \epsilon_{unc}^h + w_h \cdot \epsilon_c^h, \quad (3)$$

where  $\hat{\epsilon}^l$  and  $\hat{\epsilon}^h$  are the low-frequency and high-frequency parts of  $\hat{\epsilon}$ , respectively. Similarly,  $\epsilon_{unc}^l$ ,  $\epsilon_{unc}^h$ ,  $\epsilon_c^l$  and  $\epsilon_c^h$  follow the same notation.

### 3.4 CA-MAPS REUTILIZATION

When applied to higher resolutions, pre-trained diffusion models often present unreasonable image structures, such as duplicated objects. To address this issue, we propose to reuse the CA-maps from the previous stage to maintain layout consistency across stages. The CA-maps represent attention weights from cross-attention interactions between spatial features and textual embeddings, effectively capturing the semantic layout of the generated images. Specifically, we average the CA-maps of all cross-attention blocks when predicting  $z_L^{s_{i-1}}$  at stage  $s_{i-1}$ . After transitioning to stage  $s_i$ , we replace the current CA-maps of each cross-attention block using its linear interpolation with the averaged CA-maps  $\overline{M}_L^{s_{i-1}}$  as follows:

$$M_t^{s_i} = (1 - w_c) \cdot M_t^{s_i} + w_c \cdot \overline{M}_L^{s_{i-1}}, \quad (4)$$

where  $M_t^{s_i}$  is the CA-maps at step  $t$  of stage  $s_i$ . In this way, FreCaS can effectively maintain content consistency and prevent unexpected objects or textures during higher-resolution image generation.

## 4 EXPERIMENTS

### 4.1 EXPERIMENTAL SETTINGS

**Implementation details.** We evaluate FreCaS on three widely-used pre-trained diffusion models: SD2.1 (Rombach et al., 2022), SDXL (Podell et al., 2023) and SD3 (Esser et al., 2024). The sizes of generated images are  $\times 4$  and  $\times 16$  the original training size. Specifically, we generate images of  $1024 \times 1024$  and  $2048 \times 2048$  for SD2.1, while  $2048 \times 2048$  and  $4096 \times 4096$  for SDXL. For SD3, we only generate images of  $2048 \times 2048$  due to the GPU memory limitation. We randomly select 10K, 5K, and 1K prompts from the LAION5B aesthetic subset for generating images of  $1024 \times 1024$ ,  $2048 \times 2048$ , and  $4096 \times 4096$ , respectively. We follow the default settings and perform a 50-step sampling process with DDIM sampler for SD2.1 and SDXL, and perform a 28-step sampling process with a flow matching based Euler solver for SD3. For  $\times 4$  experiments, we employ two sampling stages at the training size and target size, respectively. For  $\times 16$  experiments, we employ three sampling stages at the training size,  $4 \times$  training size and  $16 \times$  training size, respectively. More details can be found in Appendix B.

**Evaluation metrics.** We leverage the Fréchet Inception Distance (FID) (Heusel et al., 2017) and Inception Score (IS) (Salimans et al., 2016) to measure the quality of generated images. Following He et al. (2023), the FID is computed between the samples of training size and target size, denoted as  $FID_b$ . As suggested by Du et al. (2024), we further report  $FID_p$  and  $IS_p$ , which compute the metrics at patch level, to better evaluate the image details. The CLIP score (Radford et al., 2021) is utilized to measure the text prompt alignment of generated images. As in previous works (Zhang et al., 2023), we measure the model latency on a single NVIDIA A100 GPU with a batch size of 1. We generate five images and report the averaged latency of the last three images for all methods.

### 4.2 EXPERIMENTS ON SD2.1 AND SDXL

For experiments on SD2.1, we compare FreCaS with DirectInference, MultiDiffusion (Bar-Tal et al., 2023), AttnEntropy (Jin et al., 2024), ScaleCrafter (He et al., 2023), FouriScale (Linjiang Huang, 2024) and HiDiffusion (Zhang et al., 2023). For experiments on SDXL, we compare with DirectInference, AttnEntropy, ScaleCrafter, FouriScale, HiDiffusion, AccDiffusion (Lin et al., 2024) and DemoFusion (Du et al., 2024).

Table 1: Experiments on  $\times 4$  and  $\times 16$  generation of SD2.1 and SDXL. “DO” means “duplicated object”, which indicates whether the method takes the duplicated object problem into consideration. “SpeedUP” denotes the efficiency speed-up over the DirectInference baseline. The **red** and **blue** indicate the best and second one among all methods that consider the duplicated object problem.

/	/	Methods	DO	FID <sub>b</sub> ↓	FID <sub>p</sub> ↓	IS↑	IS <sub>p</sub> ↑	CLIP SCORE↑	Latency(s)↓	SpeedUP↑
SD2.1	$\times 4$	DirectInference	✗	34.54	23.84	15.00	17.26	32.01	5.50	1x
		MultiDiffusion	✗	22.44	14.68	17.46	18.29	32.49	120.21	0.046×
		AttnEntropy	✓	30.63	<b>21.34</b>	15.67	<b>17.71</b>	32.28	5.56	0.99×
		ScaleCrafter	✓	<b>13.18</b>	22.44	<b>17.42</b>	<b>16.29</b>	<b>32.88</b>	6.36	0.86×
		FouriScale	✓	15.33	23.26	17.11	15.57	<b>32.92</b>	11.06	0.50×
		HiDiffusion	✓	16.21	25.26	17.13	16.12	32.37	<b>3.57</b>	<b>1.54×</b>
		<b>Ours</b>	✓	<b>13.14</b>	<b>21.23</b>	<b>17.55</b>	16.04	32.33	<b>2.56</b>	<b>2.16×</b>
	$\times 16$	DirectInference	✗	128.3	50.23	8.84	15.30	27.67	49.27	1×
		MultiDiffusion	✗	74.15	15.28	8.75	18.82	31.14	926.33	0.05×
		AttnEntropy	✓	127.6	<b>46.52</b>	9.31	<b>16.25</b>	28.33	49.33	1.00×
		ScaleCrafter	✓	34.55	57.47	13.02	12.12	31.44	92.86	0.53×
		FouriScale	✓	<b>34.13</b>	58.01	12.79	13.15	<b>31.68</b>	90.13	0.55×
		HiDiffusion	✓	34.17	70.58	<b>13.49</b>	11.87	31.09	<b>18.22</b>	<b>2.70×</b>
		<b>Ours</b>	✓	<b>20.11</b>	<b>43.71</b>	<b>15.22</b>	<b>13.74</b>	<b>31.92</b>	<b>13.35</b>	<b>3.69×</b>
SDXL	$\times 4$	DirectInference	✗	43.83	29.71	11.52	14.60	32.51	34.10	1×
		AttnEntropy	✓	41.30	27.67	11.69	15.04	32.71	34.36	0.99×
		ScaleCrafter	✓	24.23	23.17	14.10	14.97	32.70	39.64	0.86×
		FouriScale	✓	26.88	27.24	13.97	14.44	32.90	66.18	0.52×
		HiDiffusion	✓	20.69	21.80	15.56	15.93	32.62	<b>18.38</b>	<b>1.86×</b>
		AccDiffusion	✓	17.62	21.11	17.07	16.15	32.66	102.46	0.33×
		DemoFusion	✓	<b>16.33</b>	<b>18.77</b>	<b>17.10</b>	<b>17.21</b>	<b>33.16</b>	83.95	0.41×
	<b>Ours</b>	✓	<b>12.63</b>	<b>17.91</b>	<b>17.18</b>	<b>17.31</b>	<b>33.28</b>	<b>13.84</b>	<b>2.46×</b>	
	$\times 16$	DirectInference	✗	151.3	62.39	6.41	11.66	28.24	312.36	1×
		AttnEntropy	✓	148.9	60.54	6.46	12.44	28.46	312.46	1.00×
		ScaleCrafter	✓	75.11	73.21	8.68	9.81	30.76	560.91	0.56×
		FouriScale	✓	77.63	84.05	8.00	9.41	30.78	534.08	0.58×
		HiDiffusion	✓	83.41	120.1	9.79	9.56	29.18	<b>101.59</b>	<b>3.07×</b>
		AccDiffusion	✓	48.15	46.07	12.11	11.75	32.26	763.23	0.41×
DemoFusion		✓	<b>44.54</b>	<b>35.52</b>	<b>12.38</b>	<b>13.82</b>	<b>33.03</b>	649.25	0.48×	
<b>Ours</b>	✓	<b>40.63</b>	<b>39.82</b>	<b>12.68</b>	<b>14.16</b>	<b>33.03</b>	<b>85.87</b>	<b>3.64×</b>		

**Quantitative results.** Table 1 presents quantitative comparisons for  $\times 4$  and  $\times 16$  generation between FreCaS and its competitors. We can see that FreCaS not only outperforms other methods on synthesized image quality but also exhibits significantly faster inference speed. In specific, FreCaS achieves the best FID<sub>b</sub> scores in all experiments of SD2.1 and SDXL, achieving clear advantages over the other methods. In terms of the IS metric, FreCaS performs the best in most cases, only slightly lagging behind DemoFusion on the  $\times 16$  experiment of SDXL. (Note that DirectInference and MultiDiffusion occasionally achieve higher FID<sub>p</sub> and IS<sub>p</sub> scores because they disregard the issue of duplicated objects.) For CLIP score, FreCaS obtains the best results on 3 out of the 4 cases, except for the less challenging  $\times 4$  generation with SD2.1.

While having superior image quality metrics, FreCaS demonstrates impressive efficiency. It shows more than 2× speedup over DirectInference on  $\times 4$  generation experiments, and shows more than 3.6× speedup on the  $\times 16$  generation experiments. DemoFusion, which is overall the second best method in terms of image quality, is significantly slower than FreCaS. Its latency is about 6× and 7.5× longer than FreCas on  $\times 4$  and  $\times 16$  experiments, respectively. On the other hand, HiDiffusion, which is the second faster method, sacrifices image quality for speed. For example, on the  $\times 16$

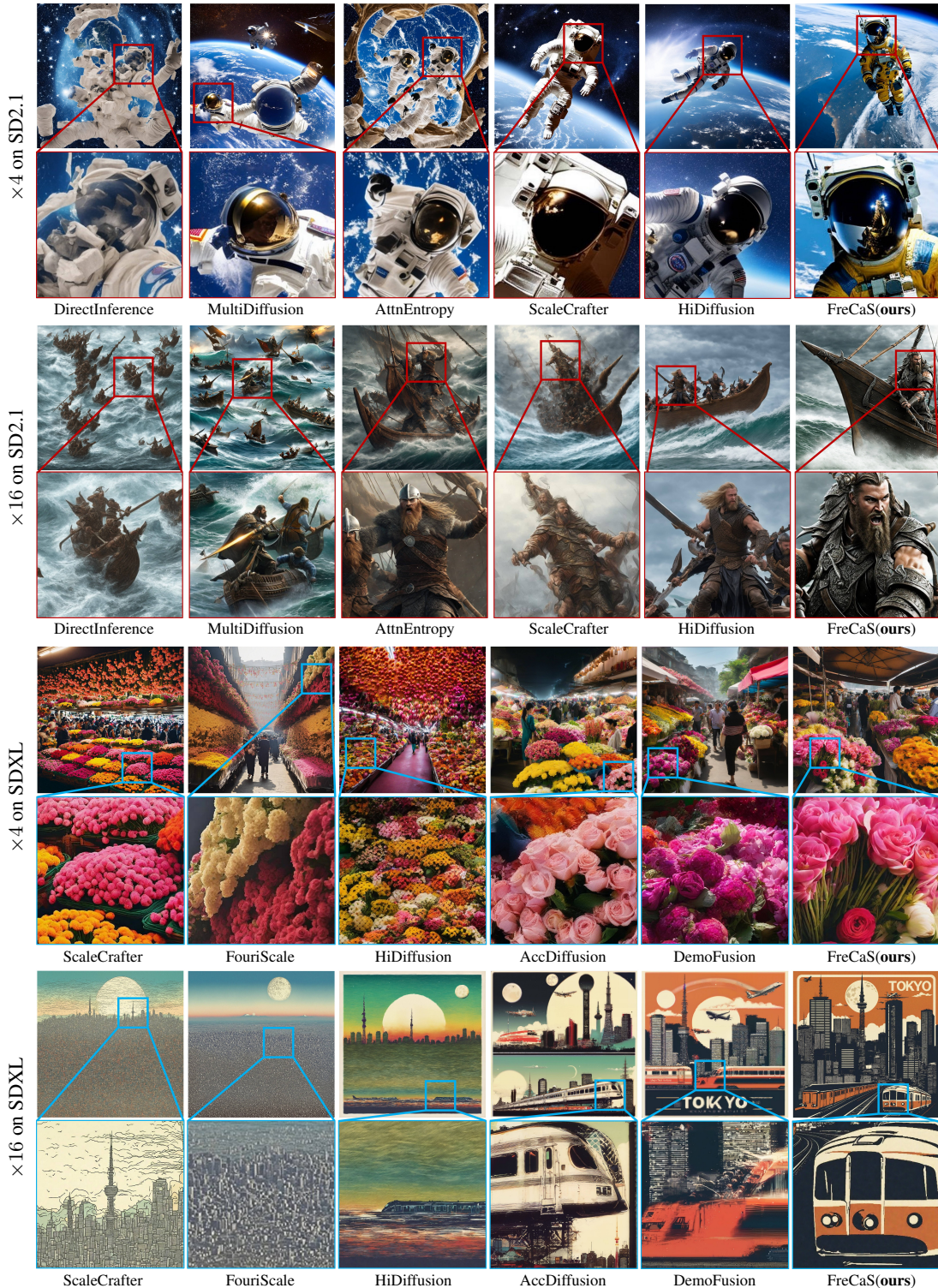


Figure 3: Visual comparison on  $\times 4$  and  $\times 16$  experiments of SD2.1 and SDXL. From top to bottom, the prompts used in the four groups of examples are: 1. "A cosmic traveler, floating in zero gravity, spacesuit reflecting the Earth below, stars twinkling in the distance." 2. "A fierce Viking, axe in hand, leading a raid, the longship slicing through the waves." 3. "A bustling flower market, stalls filled with bouquets, the air thick with fragrance, people selecting their favorites." 4. "Tokyo Japan Retro Skyline, Airplane, Railroad Train, Moon etc. - Modern Postcard". Zoom-in for better view.

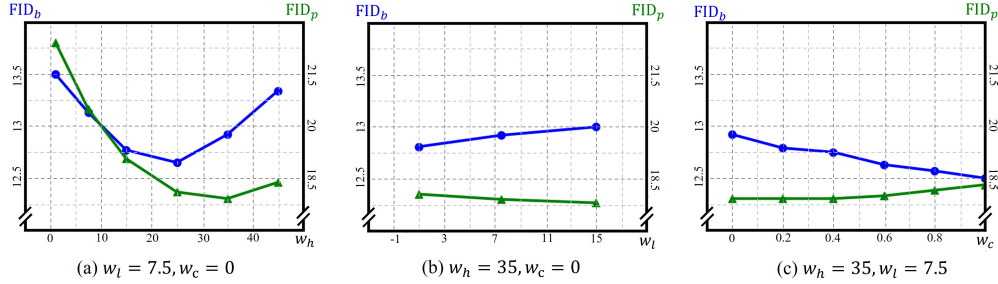


Figure 4: Ablation studies on  $w_l$  and  $w_h$  in FA-CFG strategy and  $w_c$  in CA-maps reutilization.

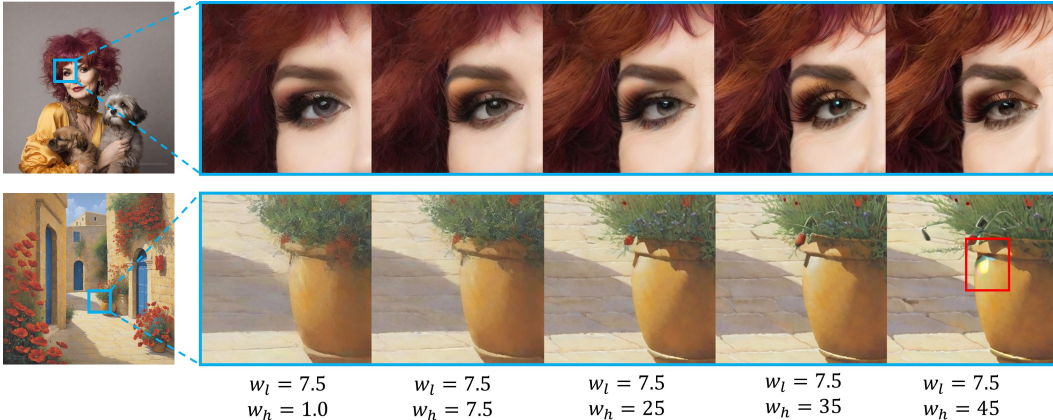


Figure 5: Visual results of adjusting  $w_h$  in the FA-CFG strategy. From top to bottom, the prompts are “Eccentric Shaggy Woman with Pet - Little Puppy” and “Rabat Painting - Mdina Poppies Malta by Richard Harpum”, respectively.

experiment with SD2.1, HiDiffusion achieves a latency of 18.22s but its FID<sub>b</sub> score is 34.17. In contrast, FreCaS is faster (13.35s) and has a much better FID<sub>b</sub> score (20.11).

**Qualitative results.** Figure 3 illustrates visual comparisons between FreCaS and competitive approaches. From top to bottom are four groups of examples, presenting the results of  $\times 4$  generation of SD2.1,  $\times 16$  generation of SD2.1,  $\times 4$  generation of SDXL, and  $\times 16$  generation of SDXL, respectively. In each group, the top row shows the generated images, while the bottom row shows the zoomed region for better observation. From Figure 3, we can see that FreCaS effectively synthesizes the described contents while maintaining a coherent scene structure. DirectInference, MultiDiffusion and AttnEntropy often produce duplicated objects, such as the many astronauts and warriors. ScaleCrafter and HiDiffusion achieve reasonable image contents in experiments of SD2.1 but generate unnatural layouts in the experiments of SDXL, such as the excessive flowers on the ceiling in  $\times 4$  experiment. Our FreCaS consistently maintains coherent image contents and layout in experiments of both SD2.1 and SDXL. AccDiffusion and DemoFusion also achieve natural image contents, but FreCaS generates clearer details such as the flowers and trains. Please refer to Appendix C for more visual results, including images with other aspect ratios.

### 4.3 EXPERIMENTS ON SD3

SD3 (Esser et al., 2024) adopts a rather different network architecture from SD2.1 and SDXL, and many existing methods cannot be applied. We can only compare FreCaS with DirectInference and DemoDiffusion Du et al. (2024). Due to page limitation, please refer to Appendix D for the results.

### 4.4 ABLATION STUDIES

In this section, we conduct ablation studies on the  $\times 4$  experiments of SDXL to investigate the settings of the FA-CFG strategy, the CA-maps re-utilization and the inference schedule of FreCaS.

**FA-CFG strategy.** The FA-CFG strategy aims to guide the model to generate content within the expanded frequency band. To achieve this, FA-CFG introduces two parameters,  $w_l$  and  $w_h$ , to adjust the guidance strength on the low and high frequency components, respectively. When  $w_l =$

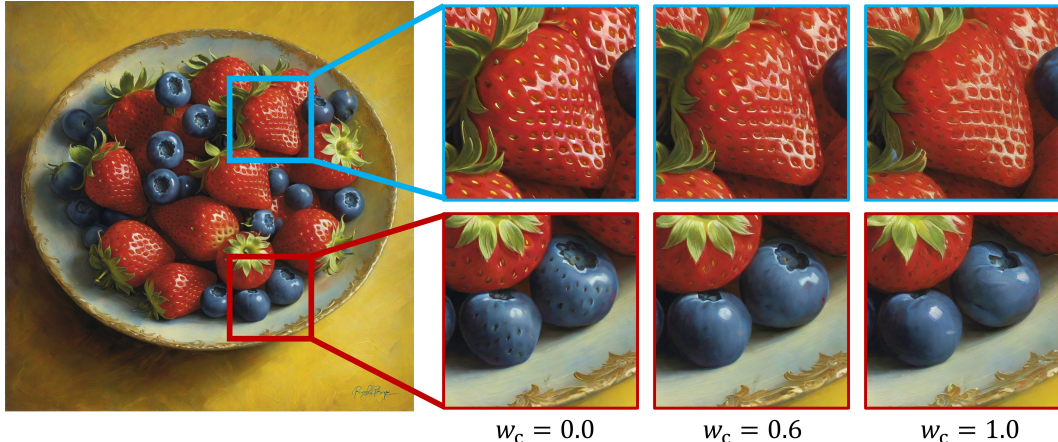


Figure 6: Visual results on adjusting  $w_c$  in CA-maps reutilization. The prompt is “Blueberries and Strawberries Art Print”.

$w_h$ , the FA-CFG strategy degenerates to the conventional CFG approach. We conduct a series of experiments to explore the optimal settings of the two parameters. First, we fix  $w_l$  at 7.5 and vary  $w_h$ . The results are shown in Figure 4(a). We observe that as  $w_h$  increases from 1.0 to 45, the  $FID_b$  and  $FID_p$  metrics initially decrease, indicating improved image quality. However, as  $w_h$  becomes too high, the metrics begin to deteriorate. The sweet spot lies between 25 and 35, achieving a low  $FID_b$  of nearly 12.65 and a low  $FID_p$  of 17.91. We then fix  $w_h$  at 35 and vary  $w_l$ . The results are presented in Figure 4(b). Reducing  $w_l$  below 7.5 leads to a slight increase in  $FID_p$  from 17.91 to 18.06, whereas increasing  $w_l$  over 7.5 deteriorates  $FID_r$  from 12.81 to 13.00. Compared to  $w_h$ , adjusting  $w_l$  brings much smaller effects on those two metrics. Thus, we set  $w_l$  to 7.5 for experiments on SD2.1 and SDXL, and set it to 7.0 for SD3.

Figure 5 provides visual examples of adjusting  $w_h$ . Increasing  $w_h$  enhances the sharpness of details, such as clearer hair strands and more vivid flower petals. However, an excessively high value of  $w_h$  (e.g., 45) will introduce artifacts, as highlighted by the red boxes in the figure. This underscores the importance of selecting an appropriate  $w_h$  value to strike a balance between detail enhancement and artifact suppression. Based on these findings, we set  $w_l$  to 7.5 and  $w_h$  to 35 yields favorable outcomes in most of the cases.

**CA-maps re-utilization.** To evaluate the effect of weight  $w_c$  in the re-utilization of CA-maps, we conduct an ablation study by varying  $w_c$  from 0 to 1. The results are shown in Figure 4(c). Increasing  $w_c$  continuously decreases  $FID_b$  but increases  $FID_p$ , indicating an improvement on the image layout but a drop on image details. To balance between the two metrics, we set  $w_c = 0.6$ . A visual example is shown in Figure 6. We see that this setting leads to a clearer textures on strawberry compared to  $w_c = 1.0$  and prevents the unreasonable surface of the blueberry in  $w_c = 0.0$ .

**Inference schedule.** FreCaS uses two factors to adjust the inference schedule. The first one is the count of additional stages  $N$ . The second factor is the timestep  $L$  of last latent in each stage. We conduct experiments on the selection of these two factors. The details can be found in Appendix E. Based on results, we set  $L$  to 200, and set  $N$  to 2 for  $\times 4$  experiments and 3 for  $\times 16$  experiments.

## 5 CONCLUSION

We developed a highly efficient **F**requency-aware **C**ascaded **S**ampling framework, namely **FreCaS**, for training-free higher-resolution image generation. FreCaS leveraged the coarse-to-fine nature of latent diffusion process, reducing unnecessary computations in processing premature high-frequency details. Specifically, we divided the entire sampling process into several stages having increasing resolutions and expanding frequency bands, progressively generating image contents of higher frequency details. We presented a **F**requency-Aware **C**lassifier-Free **G**uidance (**FA-CFG**) strategy to enable diffusion models effectively adding details of the expanded frequencies, leading to clearer textures. In addition, we fused the cross-attention maps of previous stages and current one to maintain consistent image layouts across stages. FreCaS demonstrated advantages over previous methods in both image quality and efficiency. In particular, with SDXL, it can generate a high quality  $4096 \times 4096$  resolution image in 86 seconds on an A100 GPU.

## REFERENCES

- Omer Bar-Tal, Lior Yariv, Yaron Lipman, and Tali Dekel. Multidiffusion: Fusing diffusion paths for controlled image generation. 2023.
- Junsong Chen, Jincheng Yu, Chongjian Ge, Lewei Yao, Enze Xie, Yue Wu, Zhongdao Wang, James Kwok, Ping Luo, Huchuan Lu, et al. Pixart- $\alpha$ : Fast training of diffusion transformer for photorealistic text-to-image synthesis. *arXiv preprint arXiv:2310.00426*, 2023.
- Ting Chen. On the importance of noise scheduling for diffusion models. *arXiv preprint arXiv:2301.10972*, 2023.
- Prafulla Dhariwal and Alexander Nichol. Diffusion models beat gans on image synthesis. *Advances in neural information processing systems*, 34:8780–8794, 2021.
- Ruoyi Du, Dongliang Chang, Timothy Hospedales, Yi-Zhe Song, and Zhanyu Ma. Demofusion: Democratising high-resolution image generation with no \$\$\$\$. In *Proceedings of the IEEE/CVF Conference on Computer Vision and Pattern Recognition*, pp. 6159–6168, 2024.
- Patrick Esser, Sumith Kulal, Andreas Blattmann, Rahim Entezari, Jonas Müller, Harry Saini, Yam Levi, Dominik Lorenz, Axel Sauer, Frederic Boesel, et al. Scaling rectified flow transformers for high-resolution image synthesis. In *Forty-first International Conference on Machine Learning*, 2024.
- Jiatao Gu, Shuangfei Zhai, Yizhe Zhang, Miguel Ángel Bautista, and Joshua M Susskind. f-dm: A multi-stage diffusion model via progressive signal transformation. In *The Eleventh International Conference on Learning Representations*, 2023.
- Yingqing He, Shaoshu Yang, Haoxin Chen, Xiaodong Cun, Menghan Xia, Yong Zhang, Xintao Wang, Ran He, Qifeng Chen, and Ying Shan. Scalecrafter: Tuning-free higher-resolution visual generation with diffusion models. In *The Twelfth International Conference on Learning Representations*, 2023.
- Martin Heusel, Hubert Ramsauer, Thomas Unterthiner, Bernhard Nessler, and Sepp Hochreiter. Gans trained by a two time-scale update rule converge to a local nash equilibrium. *Advances in neural information processing systems*, 30, 2017.
- Jonathan Ho and Tim Salimans. Classifier-free diffusion guidance. *arXiv preprint arXiv:2207.12598*, 2022.
- Jonathan Ho, Ajay Jain, and Pieter Abbeel. Denoising diffusion probabilistic models. *Advances in neural information processing systems*, 33:6840–6851, 2020.
- Jonathan Ho, Chitwan Saharia, William Chan, David J Fleet, Mohammad Norouzi, and Tim Salimans. Cascaded diffusion models for high fidelity image generation. *Journal of Machine Learning Research*, 23(47):1–33, 2022.
- Emiel Hooeboom, Jonathan Heek, and Tim Salimans. simple diffusion: End-to-end diffusion for high resolution images. In *International Conference on Machine Learning*, pp. 13213–13232. PMLR, 2023.
- Zhiyu Jin, Xuli Shen, Bin Li, and Xiangyang Xue. Training-free diffusion model adaptation for variable-sized text-to-image synthesis. *Advances in Neural Information Processing Systems*, 36, 2024.
- Diederik Kingma, Tim Salimans, Ben Poole, and Jonathan Ho. Variational diffusion models. *Advances in neural information processing systems*, 34:21696–21707, 2021.
- Zhihang Lin, Mingbao Lin, Meng Zhao, and Rongrong Ji. Accdiffusion: An accurate method for higher-resolution image generation. *arXiv preprint arXiv:2407.10738*, 2024.
- Aiping Zhang Guanglu Song Si Liu Yu Liu Hongsheng Li Linjiang Huang, Rongyao Fang. Fouryscale: A frequency perspective on training-free high-resolution image synthesis. *arxiv*, 2024.

- Yaron Lipman, Ricky TQ Chen, Heli Ben-Hamu, Maximilian Nickel, and Matt Le. Flow matching for generative modeling. *arXiv preprint arXiv:2210.02747*, 2022.
- Xingchao Liu, Chengyue Gong, and Qiang Liu. Flow straight and fast: Learning to generate and transfer data with rectified flow. *arXiv preprint arXiv:2209.03003*, 2022.
- Dustin Podell, Zion English, Kyle Lacey, Andreas Blattmann, Tim Dockhorn, Jonas Müller, Joe Penna, and Robin Rombach. Sdxl: Improving latent diffusion models for high-resolution image synthesis. *arXiv preprint arXiv:2307.01952*, 2023.
- Alec Radford, Jong Wook Kim, Chris Hallacy, Aditya Ramesh, Gabriel Goh, Sandhini Agarwal, Girish Sastry, Amanda Askell, Pamela Mishkin, Jack Clark, et al. Learning transferable visual models from natural language supervision. In *International conference on machine learning*, pp. 8748–8763. PMLR, 2021.
- Severi Rissanen, Markus Heinonen, and Arno Solin. Generative modelling with inverse heat dissipation. In *The Eleventh International Conference on Learning Representations*, 2023.
- Robin Rombach, Andreas Blattmann, Dominik Lorenz, Patrick Esser, and Björn Ommer. High-resolution image synthesis with latent diffusion models. In *Proceedings of the IEEE/CVF conference on computer vision and pattern recognition*, pp. 10684–10695, 2022.
- Chitwan Saharia, William Chan, Saurabh Saxena, Lala Li, Jay Whang, Emily L Denton, Kamyar Ghasemipour, Raphael Gontijo Lopes, Burcu Karagol Ayan, Tim Salimans, et al. Photorealistic text-to-image diffusion models with deep language understanding. *Advances in neural information processing systems*, 35:36479–36494, 2022.
- Tim Salimans, Ian Goodfellow, Wojciech Zaremba, Vicki Cheung, Alec Radford, and Xi Chen. Improved techniques for training gans. *Advances in neural information processing systems*, 29, 2016.
- Jiayan Teng, Wendi Zheng, Ming Ding, Wenyi Hong, Jianqiao Wangni, Zhuoyi Yang, and Jie Tang. Relay diffusion: Unifying diffusion process across resolutions for image synthesis. 2024.
- Shen Zhang, Zhaowei Chen, Zhenyu Zhao, Zhenyuan Chen, Yao Tang, Yuhao Chen, Wengang Cao, and Jiajun Liang. Hidiffusion: Unlocking high-resolution creativity and efficiency in low-resolution trained diffusion models. *arXiv preprint arXiv:2311.17528*, 2023.

# Appendix to “FreCaS: Efficient Higher-Resolution Image Generation via Frequency-aware Cascaded Sampling”

In this appendix, we provide the following materials:

- A Details of timestep shifting in the transition process (referring to Sec. 3.2 in the main paper);
- B The detailed settings of FreCaS on  $\times 4$  and  $\times 16$  generation for SD2.1, SDXL and SD3 (referring to Sec. 4.1 in the main paper);
- C More visual results and visual comparisons (referring to Sec. 4.2 in the main paper);
- D Experimental results of generation of SD3 (referring to Sec. 4.3 in the main paper);
- E Ablation studies on inference schedule (referring to Sec. 4.4 in the main paper);

## A SHIFTING TIMESTEP IN THE TRANSITION PROCESS

As mentioned in Sec. 3.2 of the main paper, FreCaS employs a five-step transition process to transform the last latent in the current stage  $z_L^{s_{i-1}}$  to the first latent in the next stage  $z_F^{s_i}$ . In addition to changing the resolution, we adjust the timestep from  $L$  to  $F$  to ensure that the signal-to-noise ratio (SNR) (Kingma et al., 2021) could be a constant in the transition process. Given a state  $z_t = \sqrt{\alpha_t}z_0 + \sqrt{1 - \alpha_t}\epsilon$  at timestep  $t$ , the SNR is defined as  $\text{SNR}(z_t) = \frac{\alpha_t}{1 - \alpha_t}$ , where  $\alpha_1, \dots, \alpha_T$  represent the noise schedule, and  $\epsilon$  is Gaussian noise. It has been found (Hoogeboom et al., 2023; Chen, 2023) that the SNR maintains a consistent ratio across resolutions for diffusion models using the same noise schedule:

$$\text{SNR}(z_t^s) = \text{SNR}(z_t^{\hat{s}}) \cdot \left(\frac{s}{\hat{s}}\right)^\gamma,$$

where  $s$  and  $\hat{s}$  denote different resolutions. The value of  $\gamma$  is typically set to 2.

Teng et al. (2024) and Gu et al. (2023) proposed to redesign the noise schedule to keep SNR consistent when changing the resolutions of intermediate states. Since the pre-trained diffusion models have fixed noise schedules, in this paper we adjust the timestep, instead of the noise schedule, to ensure consistent SNR between  $z_L^{s_{i-1}}$  and  $z_F^{s_i}$ :

$$\text{SNR}(z_L^{s_{i-1}}) = \text{SNR}(z_F^{s_i}) \Rightarrow F = \alpha^{-1} \left( \frac{\left(\frac{s_{i-1}}{s_i}\right)^\gamma \cdot \alpha_L}{1 + \left(\left(\frac{s_{i-1}}{s_i}\right)^\gamma - 1\right) \cdot \alpha_L} \right), \quad (5)$$

where  $\alpha^{-1}$  is the inverse function of  $\alpha_t$ . Proper adjustment of  $\gamma$  can yield additional improvements.

Besides, SD3 (Esser et al., 2024) employs a similar formula to shift the timestep when varying resolutions:

$$F = \frac{\sqrt{\frac{s_i}{s_{i-1}}} \cdot L}{1 + \left(\sqrt{\frac{s_i}{s_{i-1}}} - 1\right) \cdot L}. \quad (6)$$

## B EXPERIMENTAL SETTING DETAILS

The experimental setting details of our FreCaS are listed in Table 2.

## C MORE VISUAL RESULTS

### C.1 MORE VISUAL RESULTS

Figure 7 illustrates more visual results of FreCaS, including those with varying aspect ratios. From top to bottom, and left to right, the prompts used in examples are: 1. “Beautiful winter wallpapers.” 2. “A regal queen adorned with jewels.” 3. “A majestic phoenix, wings ablaze, rising from ashes, the flames casting a warm glow.” 4. “Lady in Red oil portrait painting won the John Singer Sargent

Table 2: Detailed settings of FreCaS on the experiments.  $N$  denotes the count of additional stages. “Steps” presents the sampling steps in each stage.  $L$  presents the timestep of last latent in each stage except for the final one.  $\gamma$  denotes the SNR ratio in the transition process.  $w_l$ ,  $w_h$  and  $w_c$  are the hyper-parameters of the proposed FA-CFG and CA-maps re-utilization.

		$N + 1$	Steps	$L$	$\gamma$	$w_l$	$w_h$	$w_c$
SD2.1	$\times 4$	2	40,10	100	3.0	7.5	45.0	0.6
	$\times 16$	3	30,10,10	200,200	3.0	7.5	35.0	0.4
SDXL	$\times 4$	2	40,10	200	1.5	7.5	35.0	0.6
	$\times 16$	3	30,5,15	400,200	2.0	7.5	35.0	0.6
SD3	$\times 4$	2	20,8	50	-	7.0	35.0	0.5

Table 3: Experiments on  $\times 4$  generation of SD3.

Methods	FID $_b$ ↓	FID $_p$ ↓	IS↑	IS $_p$ ↑	CLIP SCORE↑	Latency (s)↓	SpeedUP↑
DirectInference	35.68	45.35	12.52	12.60	31.45	38.53	1×
Demodiffusion	15.19	44.34	17.84	14.99	31.09	63.33	0.61×
<b>Ours</b>	9.76	26.62	17.83	16.72	31.17	15.94	2.42×

People’s award.” 5. “Star of the day – Actress Evelyn Laye - 1917.” 6. “Photograph - Clouds Over Daicey Pond by Rick Berk.” 7. “little-boy-with-large-bulldog-in-a-garden-france.” 8. “03-Brussels-Maja-Wronska-Travels-Architecture-Paintings.”, 9. “Red Fox Pup Print by William H. Mullins.” 10. “Lovely Illustrations Of Cityscapes Inspired By Southeast Asia Malaysian digital illustrator Chong Fei Giap’s illustrations of cityscapes are lovely and inspiring. Fantasy Landscape, Landscape Art, Illustrator, Japon Tokyo, Animation Background, Art Background, Matte Painting, Anime Scenery, Jolie Photo.” 11. “A plate with creamy chicken and vegetables, a side of onion rings, a cup of coffee and a slice of cheesecake.” 12. “Hyper-Realistic Portrait of Redhead Girl Drawn with Bic Pens.”

## C.2 MORE VISUAL COMPARISONS

We show more visual comparisons in Figure 8. From top to bottom, the prompts used in the four groups of examples are: 1. “A small den with a couch near the window.” 2. “A painting of a candlestick holder with a candle, several pieces of fruit and a vase, with a gold frame around the painting.” 3. “A noble knight, riding a white horse, the castle gates opening.” 4. “Mystical Landscape Digital Art - Lonely Tree Idyllic Winterlandscape by Melanie Viola.”

## D EXPERIMENTS ON SD3

In this section, we present the results of the  $\times 4$  generation experiments on SD3. SD3 employs a transformer-based denoising network. It eliminates all convolutional layers, thereby preventing the application of many existing methods, such as ScaleCrafter and FouriScale. Besides, SD3 exhibits fine details in the central region but shows corrupted textures in the surrounding regions (see Figure 9). This issue with the image layout also significantly impacts the performance of other methods, such as DemoFusion. Therefore, we only compare our FreCaS with DirectInference and DemoFusion. Table 3 and Figure 9 present the quantitative and qualitative results, respectively.

From Table 3, it is evident that FreCaS achieves superior performance in terms of image quality and inference speed. Specifically, FreCaS achieves the best results on FID $_b$ , FID $_p$ , IS, and IS $_p$ , and only slightly lags behind DirectInference in terms of CLIP score. Moreover, FreCaS generates a  $2048 \times 2048$  image in about 16 seconds, achieving a speed-up of 2.42× and 3.97× compared to DirectInference and DemoFusion, respectively. Figure 9 illustrates the generated images. Directly employing the pre-trained SD3 model to generate higher-resolution images, DirectInference leads



Figure 7: Visual results of FreCaS on SDXL. Please zoom-in for better view.

to unreasonable image layout with the surrounding parts being corrupted, such as the road and trees. The results of DemoFusion exhibits strange artifacts, such as the car faces and eyes. In contrast, our FreCaS successfully maintains the natural image structure while obtaining fine details.

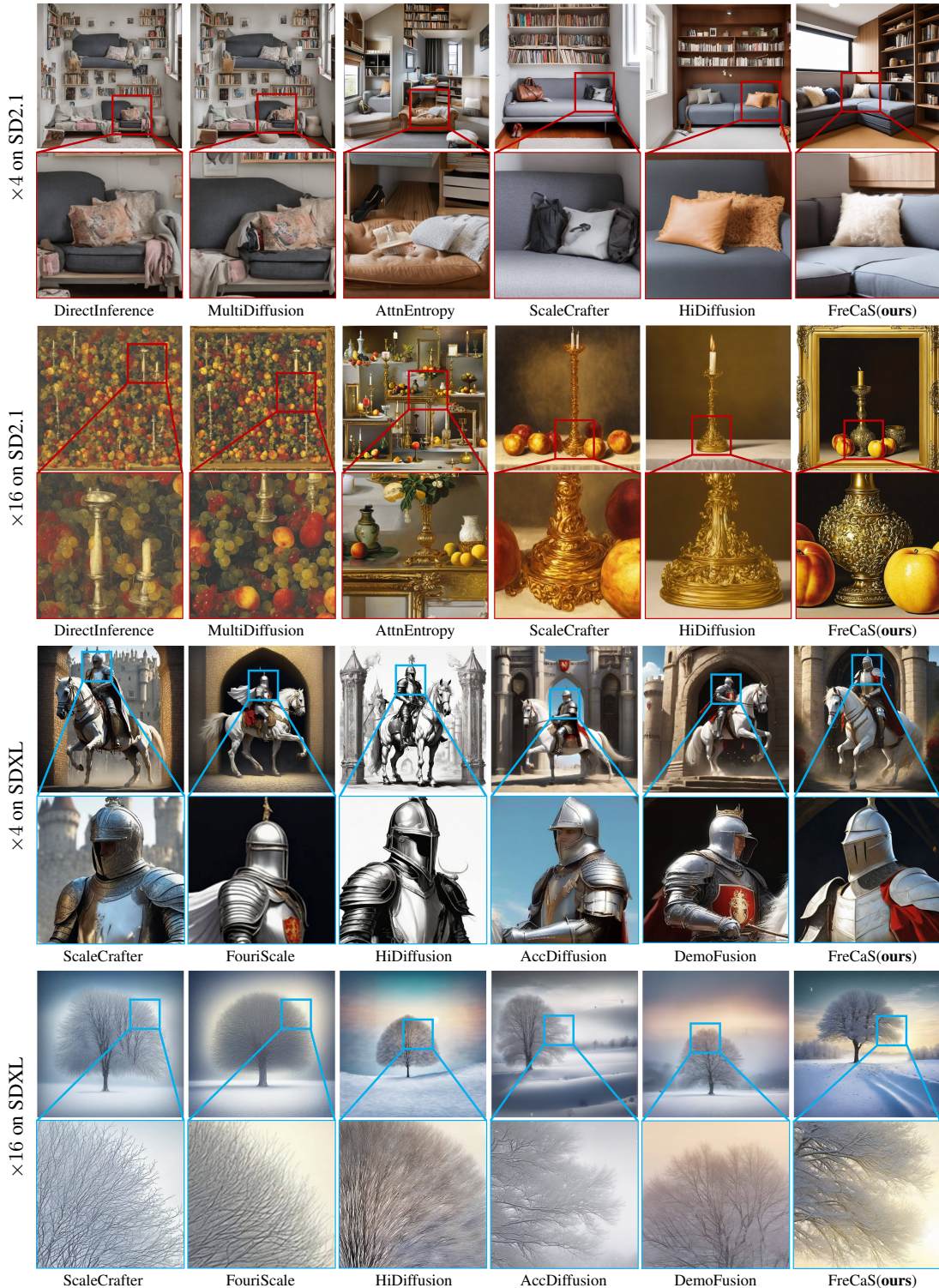


Figure 8: Visual comparisons on  $\times 4$  and  $\times 16$  experiments of SD2.1 and SDXL. Please zoom-in for better view.

## E ABLATION STUDIES ON INFERENCE SCHEDULE

In this section, we conduct experiments on the selection of  $N$  (number of additional stages) and  $L$  (the timestep of last latent in each stage). The two factors are employed to adjust the inference

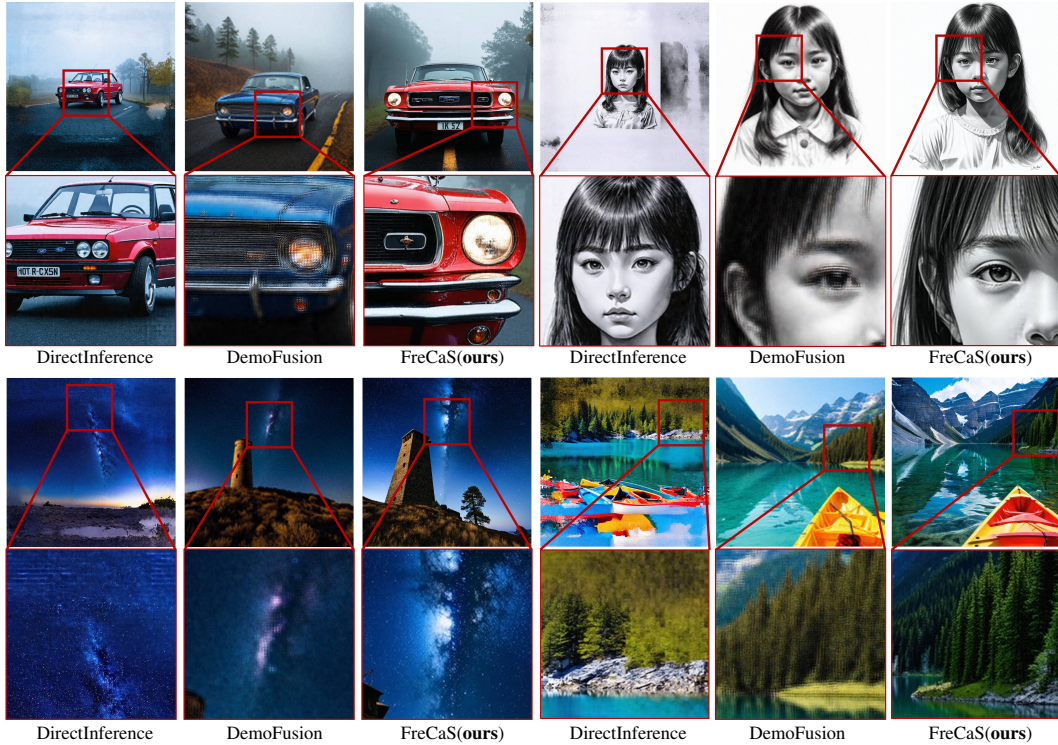


Figure 9: Visual comparison on  $\times 4$  experiments of SD3. From top to bottom, from left to right, the prompts used in the four groups of examples are: 1. “Car Photograph - Ford In The Fog by Debra and Dave Vanderlaan.” 2. “Rupert Young is Sir Leon in Merlin season 5 copy.” 3. “Watchtower, Shooting Star & Milky Way, Gualala, CA.” 4. “Colorful Autumn in Mount Fuji, Japan - Lake Kawaguchiko is one of the best places in Japan to enjoy Mount Fuji scenery of maple leaves changing color giving image of those leaves framing Mount Fuji.”. Zoom-in for better view.

Table 4: Ablation studies on  $N$  in FreCaS.

$N$	resolutions	$FID_b \downarrow$	$FID_p \downarrow$
0	2048	43.83	29.71
1	1024 $\rightarrow$ 2048	12.63	17.91
2	1024 $\rightarrow$ 1536 $\rightarrow$ 2048	41.36	28.68

Table 5: Ablation studies on  $L$  in FreCaS.

$L$	$FID_b \downarrow$	$FID_p \downarrow$
0	12.57	18.20
100	12.69	18.10
200	12.63	17.91
300	13.30	18.57
400	13.34	18.62

schedule of our FreCaS. We reports the scores of  $FID_b$  and  $FID_p$  by varying the two factors in Table 4 and Table 5, respectively.

**Choice of  $N$ .** From Table 4, we see that  $N = 1$  achieves an  $FID_b$  score of 12.63 and an  $FID_p$  score of 17.91, significantly better than  $N = 0$  and  $N = 2$  in the  $\times 4$  generation task for SDXL. This could be attributed to the fact that a larger value of  $N$  introduces more transition steps, which

can lead to much information loss. Conversely, a smaller value of  $N$  reduces the effectiveness of FreCaS, degenerating it to the DirectInference method.

**Choice of  $L$ .** From Table 5, we can see that a smaller  $L$  improves  $FID_b$  score but deteriorates  $FID_p$ . This is because the details generated at lower resolutions conflict with those at higher resolutions. Thus, we set  $L$  to 200 to avoid generating excessive unwanted details in the early stages.